An Electrokinetic Study of Amino Acid and Potential-Determining Ions for Enhanced Waterflooding in Carbonate Reservoirs

Ricardo A. Lara Orozco[1], Gayan Aruna Abeykoon[1], Ryosuke Okuno[1]*, and Larry W. Lake[1]

[1]The University of Texas at Austin

Summary

Reservoir rock wettability plays an important role in waterflooding especially in fractured carbonate reservoirs because oil recovery tends to be inefficient from the mixed-wet or oil-wet rock matrix. Improved oil recovery has been observed by adjusting the concentrations of potential-determining ions (PDIs) to alter the wettability of carbonate rocks.

Our previous study showed that the oil recovery from carbonate reservoirs by waterflooding can be enhanced by the addition of glycine, the simplest amino acid. The interaction of glycine anion and oil-wet carbonate surfaces was confirmed in contact angle measurements and yielded the incremental oil recovery in imbibition experiments. This paper presents a surface complexation model (SCM) for the interaction between glycine and oil-wet carbonate surfaces that considers the impact of temperature, pH, salinity, and the concentrations of PDIs.

The proposed SCM was tuned based on the zeta potential (ZP) data reported for synthetic calcite in glycine solutions. The tuned model predicts that the strong affinity of glycine for the oil-wet carbonate surface causes the carboxylic acids to desorb from the surface. The concentration of adsorbed carboxylic acids was in qualitative agreement with the water-wetting state of carbonate rocks inferred from the reported contact angle and spontaneous imbibition experiments. Moreover, the model indicates that glycine's performance as a wettability alteration agent improves significantly at high temperatures. It also suggests that enhanced oil recovery (EOR) by formation brine (FB) with 1 to 3 wt% glycine at high temperatures should be similar to the injection of low-salinity seawater (LSW). The proposed SCM supports glycine's potential to change the wettability of oil-wet carbonates at high salinity, high hardness, and high temperature.

Introduction

Tuning the brine composition and salinity has been investigated for EOR in carbonate reservoirs, mainly because of its lower cost and minimal environmental impact in comparison to other EOR methods. The increased oil recovery observed in many laboratory experiments has been attributed to the alteration of the rock wettability to a less-oil-wetting state that changes the relative permeabilities and the capillary pressures to more favorable values. The consensus in the literature is that the electrokinetic behavior of carbonate rocks can be used as a surrogate of their wetting state, as observed by combining ZP and contact angle measurements with imbibition and coreflooding experiments (Myint and Firoozabadi 2015; Hao et al. 2019; Liu and Wang 2020). Hence, the wettability alteration of carbonate rocks has been related to the rock surface potential alteration by the combined effect of the brine pH, salinity, and concentration of PDIs.

Lara Orozco et al. (2020) demonstrated the wettability alteration by the addition of amino acids to the original FB or low-salinity brine. Glycine, the simplest amino acid, showed promising results in contact angle and imbibition experiments using FB, seawater (SW), and 10-times-diluted SW. The main advantages of glycine are that it is nontoxic, environmentally friendly, and commercially available at a low cost (Tripathy et al. 2018) and that it is stable in high-salinity and high-hardness brine at high temperatures (Lara Orozco et al. 2020).

The hypothesis behind the observed wettability alteration by glycine is that its anionic form interacts with the oil-wet carbonate surface, releasing the adsorbed organic acids from the surface. This interaction is influenced by temperature and the overall charge of both glycine and the carbonate surface, both of which are sensitive to pH. Besides, the solution pH, the brine salinity, and the concentration of PDIs affect the surface charge of the carbonate surface, as well as the glycine aqueous speciation. Therefore, the potential of glycine to alter the wettability of carbonate could be enhanced or diminished based on the brine pH, composition, and salinity.

The objective of this research was to investigate the impact of glycine on the wetting state of carbonate rocks through an SCM. The SCM in this research includes the aqueous and surface complexation of the PDIs: Ca^{2+}, Mg^{2+}, SO_4^{2-}, and CO_3^{2-}as proposed in Brady et al. (2012). The rock's wetting state was considered a function of the amount of adsorbed carboxylic acid as in Eftekhari et al. (2017). The main novelty of this research lies in the inclusion of glycine surface complexation with calcite and the formation of aqueous complexes with Ca^{2+} and Mg^{2+} while considering the impact of brine salinity and temperature on glycine speciation. The estimated wettability from the SCM was analyzed and compared with the contact angle and spontaneous-imbibition experiments with glycine as reported in Lara Orozco et al. (2020).

Method

This section first presents the SCM of calcite. Then, the addition of glycine's aqueous and surface complexation to calcite's SCM and the modeling of wettability alteration are discussed. The resulting geochemical model was implemented in the open-source, geochemical solver PHREEQC v3.6.2 (Parkhurst 1995) developed by the United States Geological Survey (USGS).

*Corresponding author; email: okuno@utexas.edu

This paper (SPE 201482) was accepted for presentation at the SPE Annual Technical Conference and Exhibition, Virtual, 26–29 October 2020, and revised for publication. Original manuscript received for review 9 June 2021. Revised manuscript received for review 14 September 2021. Paper peer approved 15 September 2021.

Calcite's SCM. The first SCM for calcite was proposed by Van Cappellen et al. (1993) based on the analogous aqueous complexation reactions and then augmented for the adsorption of Mg^{2+} and SO_4^{2-} (Pokrovsky and Schott 2002; Hiorth et al. 2010; Brady et al. 2012). In this research, the equilibrium constants proposed by Brady et al. (2012) were considered as the base case (**Table 1**) as it has been used in many studies on LSW [e.g., Qiao et al. (2016), Sanaei et al. (2019), Tetteh et al. (2020), and Bordeaux-Rego et al. (2021)]. The following sections describe in detail the surface and aqueous complexation reactions, and the electric double layer model considered in this study.

No.	Surface Complexation Reaction	$\log_{10}K$ (25°C)	ΔH_R (kJ/mol)
S1	$>CaOH_2^+ \iff >CaOH + H^+$	−11.85	68.82
S2	$>CaOH_2^+ + SO_4^{2-} \iff >CaSO_4^- + H_2O$	2.10	29.81
S3	$>CaOH_2^+ + CO_3^{2-} \iff >CaCO_3^- + H_2O$	4.53	14.90
S4	$>CO_3^- + H^+ \iff >CO_3H$	5.10	12.71
S5	$>CO_3^- + Ca^{2+} \iff >CO_3Ca^+$	2.50	14.02
S6	$>CO_3^- + Mg^{2+} \iff >CO_3Mg^+$	2.50	14.90

Table 1—Calcite's surface complexation reactions. The equilibrium constants are from Brady et al. (2012) and the enthalpies of reaction are from Hiorth et al. (2010).

Surface Complexation Reactions. In the SCM, the carbonate mineral surface is represented by the hydrated calcium, $>CaOH_2^+$, and carbonate, $>CO_3^-$, surface sites, where > indicates the bonding to the mineral structure. These surface sites can be protonated and deprotonated to form >CaOH and $>CO_3H$, respectively. The primary surface sites, $>CaOH_2^+$ and $>CO_3^-$, will also form complexes with the cations and anions in the solution, Ca^{2+} , Mg^{2+} , SO_4^{2-} , and CO_3^{2-}. In this research, a surface site density of 4.95 sites/nm^2 was used for each primary species, $>CaOH_2^+$ and $>CO_3^-$ (Song et al. 2019; Tetteh et al. 2020).

The surface complexation reactions are modeled through standard mass action equations. The apparent equilibrium constant, K_{app} , comes from the product of the intrinsic equilibrium constant, K, that describes the chemical binding and a term that accounts for the electrostatic interactions between the surface and the adsorbed ion:

$$K_{app} = K \exp\left(-\frac{\Delta z F}{RT}\right), \quad (1)$$

where ψ is the surface potential (V), Δz is the net change of the surface charge caused by the formation of the surface complex, F is the Faraday's constant (96 485 C·mol^{-1}), R is the universal gas constant (8.314 J·mol^{-1}·K^{-1}), and T is the absolute temperature (K).

The surface charge density, σ (C·m^{-2}), is directly determined by adding up the charges of all the surface complexes:

$$\sigma = \frac{F}{SA}\sum_i m_{si} z_{si}, \quad (2)$$

where S is the solid concentration (g·L^{-1}), A is the solid specific surface area (m^2·g^{-1}), m_{si} and z_{si} are the concentration (mol·L^{-1}), and the electrical charge of the surface species , respectively.

The corresponding K values at 95°C were estimated using the van't Hoff equation (Appelo and Postma 2005)

$$\frac{d\ln K}{dT} = \frac{\Delta H_R}{RT^2}, \quad (3)$$

where ΔH_R is the enthalpy of reaction (J·mol^{-1}). The values of Reactions S1 to S6 in **Table 1** were estimated from the equilibrium constants reported by Hiorth et al. (2010) at 25 and 130°C assuming that the temperature dependence of the surface complexes was similar to the analogous aqueous complexes. This approach has been followed by several authors to estimate the K values of Reactions S1 to S6 at high temperatures [e.g., Brady et al. (2012), Qiao et al. (2016), Sanaei et al. (2019), and Tetteh et al. (2020)].

An important assumption when integrating Eq. 3 is that the reaction enthalpy, ΔH_R, is constant with temperature. This approximation is usually valid within a few tens of degrees (Appelo and Postma 2005). The ΔH_R of the surface complexation reactions could be obtained from ZP measurements; however, only few experimental data have been reported at high temperatures (Bonto et al. 2021). The ZP predictions at high temperatures are expected to be qualitatively correct, as the reactivity of Ca^{2+} , Mg^{2+} , and SO_4^{2-} tends to increase with temperature (Zhang et al. 2007), which corresponds to positive enthalpies of reaction (**Table 1**).

Electrical Double Layer Model. The equilibrium surface speciation depends on the surface potential (Eq. 1), while the surface speciation yields the surface charge density σ (Eq. 2). An electrical double layer model is used to calculate ψ from σ. In this research, we considered the diffused layer model (Dzombak and Morel 1990), where the charge-potential relationship was given by the Grahame equation derived from the Gouy-Chapman theory:

$$\sigma = \sqrt{8000\varepsilon_r\varepsilon_0 RTI}\sinh\left(\frac{z_\pm F}{2RT}\right), \quad (4)$$

where I is the solution ionic strength (mol·dm^{-3}), ε_r is the relative permittivity of the solution (78.5 for water at 25°C), ε_0 is the permittivity of free space (8.854×10^{-12} C·V^{-1}·m^{-1}), and z is the charge of the background solute that is assumed to be unity.

Relationship between Surface Potential and ZP. The Debye-Hückel equation is used to estimate the ZP, ζ (V), from the surface potential calculated by the SCM. This approximation is valid for surface potentials in the range of ±25 mV:

$$\zeta = \psi e^{-\kappa d_s}, \tag{5}$$

where d_s is the slip plane and κ is the inverse of the Debye length given by

$$\kappa^{-1} = \sqrt{\frac{\varepsilon_r \varepsilon_0 k_b T}{2 N_A e^2 I}}. \tag{6}$$

Here, k_b is the Boltzmann constant (1.381×10^{-23} J·K^{-1}), e is the elementary charge (1.602×10^{-19} C), N_A is the Avogadro's number (6.002×10^{23} mol^{-1}), and the other terms were previously defined.

The value of the slip plane, d_s, has been typically assumed to be 0.6 nm (Sanaei et al. 2019). In this research, we consider d_s to be a function of ionic strength as described by the correlation from Heberling et al. (2011):

$$d_s = \frac{0.13}{\sqrt{I}} (\text{nm}). \tag{7}$$

Note that the proportionality factor in Eq. 7 was incorrectly defined as 0.0013 in Heberling et al. (2011). The correct value, 0.13, was directly obtained from Fig. 12 in Heberling et al. (2011).

Aqueous Chemistry. The aqueous species considered in the model are the free ions in solution, H^+, OH^-, Na^+, Ca^{2+}, Mg^{2+}, Cl^-, SO_4^{2-}, CO_3^{2-}, and HCO_3^-, and the aqueous complexes in **Table 2.** The activity of charged aqueous species are calculated using the Truesdell and Jones equation:

$$\log \gamma_i = -\frac{A z_i^2 \sqrt{I}}{1 + B a_i \sqrt{I}} + b_i I, \tag{8}$$

No.	Aqueous Reaction	$\log_{10} K$ (25°C)
A1	$HCO_3^- \Longleftrightarrow H^+ + CO_3^{2-}$	−10.33
A2	$CO_3^{2-} \Longleftrightarrow 2H^+ + CO_2 + H_2O$	16.68
A3	$NaSO_4^- \Longleftrightarrow Na^+ + SO_4^{2-}$	−0.70
A4	$CaSO_4 \Longleftrightarrow Ca^+ + SO_4^{2-}$	−2.25
A5	$MgSO_4 \Longleftrightarrow Mg^+ + SO_4^{2-}$	−2.37
A6	$NaCO_3^- \Longleftrightarrow Na^+ + CO_3^{2-}$	−1.27
A7	$CaCO_3 \Longleftrightarrow Ca^+ + CO_3^{2-}$	−3.22
A8	$MgCO_3 \Longleftrightarrow Mg^+ + CO_3^{2-}$	−2.98
A9	$NaHCO_3 \Longleftrightarrow Na^+ + HCO_3^-$	0.25
A10	$CaHCO_3^+ \Longleftrightarrow Ca^+ + CO_3^{2-} + H^+$	−11.43
A11	$MgHCO_3^+ \Longleftrightarrow Mg^+ + CO_3^{2-} + H^+$	−11.40

Table 2—Aqueous complexation reactions from PHREEQC database.

where γ_i is the activity coefficient, I is the ionic strength, A and B are the temperature-dependent coefficients, and a_i and b_i are the ion-specific parameters defined in the PHREEQC database. Eq. 8 yields reasonable approximations of the activity coefficient of aqueous species for ionic strength values up to 2 M (Parkhurst 1990). For uncharged species, the activity coefficients depend solely on the ionic strength, I, using

$$\log \gamma_i = 0.1 I. \tag{9}$$

The equilibrium conditions with calcite were also included in the SCM calculations according to

$$CaCO_3(s) \Longleftrightarrow Ca^{2+}(aq) + CO_3^{2-}(aq), \log_{10} K = -8.48, \tag{10}$$

where the equilibrium constant is from Appelo and Postma (2005), and its temperature dependence is calculated from the analytical expression proposed in Plummer and Busenberg (1982). Equilibrium with atmospheric CO_2 was also considered in some calculations by specifying carbon dioxide partial pressure of $10^{-3.4}$atm at 20°C.

Glycine's Aqueous and Surface Reactions. This section describes the chemical reactions for the aqueous speciation of glycine. It also describes an extended van't Hoff model and a Debye-Hückel type equation to estimate the impact of salinity and temperature on glycine aqueous speciation. Finally, a surface complexation reaction is proposed to model the adsorption of glycine anion onto the surface of carbonate rocks.

Glycine's Aqueous Speciation. The carboxyl (-COOH) and amino (-NH_2) groups of amino acids can be deprotonated and protonated as a function of the solution pH. This results in the formation of the zwitterion, anion, and cation amino acid species **(Fig. 1).** The speciation of glycine is given by

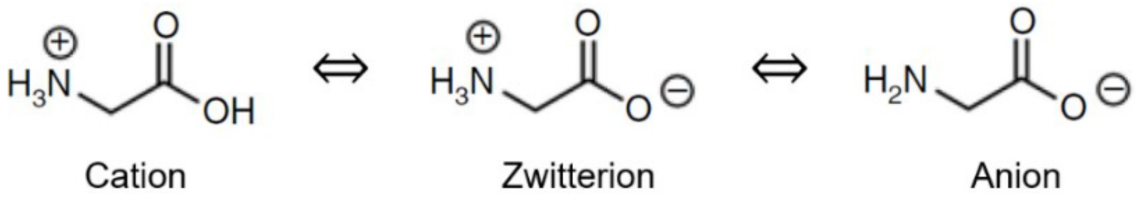

Fig. 1—Chemical structures of the cation, zwitterion (neutral), and anion species of glycine. The *K* values and the p*I* values depend on thermodynamic conditions.

$$GlyH+H^+ \Leftrightarrow GlyH_2^+, \quad (11)$$

$$GlyH \Leftrightarrow Gly^-+H^+, \quad (12)$$

where, for brevity, the zwitterion ($N^+H_3CH_2COO^-$), anion ($NH_2CH_2COO^-$), and cation ($N^+H_3CH_2COOH$) forms of glycine have been represented as GlyH, Gly^-, and $GlyH_2^+$, respectively.

The equilibrium constants for Reactions G1 and G2 in **Table 3** are well-documented in the literature at ideal conditions [i.e., room temperature (25°C) and low ionic strength solutions] (Karty 2018). However, these conditions significantly deviate from those encountered in typical waterflooding applications in carbonates (Sharma and Mohanty 2013). It is necessary to include in the model how glycine's speciation is affected by salinity, temperature, and brine composition.

	Reaction			$\log_{10}K$ (25°C)
Aqueous speciation				
G1	$GlyH + H^+$	$\Longleftrightarrow$	$GlyH_2^+$	2.34
G2	$GlyH$	$\Longleftrightarrow$	$Gly^- + H^+$	–9.78
Aqueous complexation reactions				
G3	$Gly^- + Na^+$	$\Longleftrightarrow$	$NaGly$	–0.35
G4	$Gly^- + Ca^{2+}$	$\Longleftrightarrow$	$CaGly^+$	1.40
G5	$Gly^- + Mg^{2+}$	$\Longleftrightarrow$	$MgGly^+$	2.00
G6	$GlyH + Ca^{2+}$	$\Longleftrightarrow$	$CaHGly^{2+}$	0.40
G7	$GlyH + Mg^{2+}$	$\Longleftrightarrow$	$MgHGly^{2+}$	0.40
Surface complexation reaction				
S7	$>CaOH_2^+ + Gly^-$	$\Longleftrightarrow$	$>CaGly + H_2O$	1.40

Table 3—Glycine's aqueous and surface reactions. The equilibrium constants of Reactions G1 and G2 are calculated as a function of temperature and brine salinity using Eqs. 10 and 11, respectively. The equilibrium constants for Reactions G3 to G7 are from De Stefano et al. (2000). Reaction S7 is proposed in this research based on Reaction G4.

Many studies have reported the experimental values for the equilibrium constants of Reactions G1 and G2 at temperatures up to 275°C using the calorimetry technique (Izatt et al. 1992; Gillespie et al. 1995; Wang et al. 1996; Clarke et al. 2005). Based on these data, various models have been proposed to predict the dependency of glycine's aqueous speciation on temperature (Gupta and Svendsen 2013). In this research, we considered the extended van't Hoff model proposed in Clarke et al. (2005):

$$\ln K(T) = \ln K(T_r) + \frac{\Delta H_r}{R}\left(\frac{1}{T_r}-\frac{1}{T}\right) + \frac{\Delta C_p^0}{R}\left(\ln\left(\frac{T}{T_r}\right)+\frac{T_r}{T}-1\right), \quad (13)$$

where T_r is the reference temperature (298.15 K), ΔH_r is the enthalpy of reaction at the reference temperature (J·mol^{-1}), and ΔC^0_p is the standard partial molar heat capacity of reaction (J·K^{-1}·mol^{-1}). The values reported by Clarke et al. (2005) for glycine are $\Delta H_r = 4.54$ kJ·mol^{-1} and $\Delta C^0_p = -120.9$ J·K^{-1}·mol^{-1} for K_{G1}, and $\Delta H_r = 44.4$ kJ·mol^{-1} and ΔC^0_p J·K^{-1}·mol^{-1} for K_{G2}. This model was compared with the experimental values reported in the literature at different temperatures in **Fig. 2.**

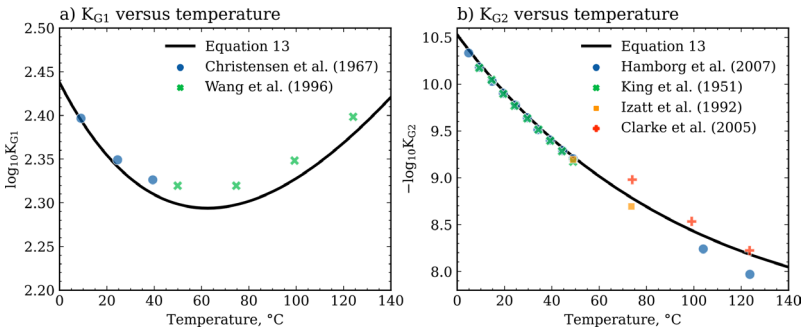

Fig. 2—Effect of temperature on the equilibrium constants for Reactions (a) G1 and (b) G2 in Table 3. The theoretical value was calculated using Eq. 13 and compared to the experimental values found in the literature. References (King 1951; Christensen et al. 1967; Izatt et al. 1992; Wang et al. 1996; Clarke et al. 2005; Hamborg et al. 2007).

In De Stefano et al. (2000), a DebyeHückel type equation was proposed to model the impact of ionic strength on glycine's aqueous speciation:

$$\log K(I) = \log K(I=0) - \frac{z^* \sqrt{I}}{2+3\sqrt{I}} + CI + D\sqrt{I^3} + EI^2, \quad (14)$$

where $z^* = \sum (\text{charges})^2_{\text{reactants}} - \sum (\text{charges})^2_{\text{products}}$ from the reactions in Eqs. 10 and 11, and C, D, E are empirical parameters, of which the values in **Table 4** were determined by De Stefano et al. (2000) from fitting their experimental data. The equilibrium constants of Reactions G1 and G2 as a function of ionic strength predicted by Eq. 11 are in good agreement with the experimental data compiled by Kiss et al. (1991) **(Fig. 3).**

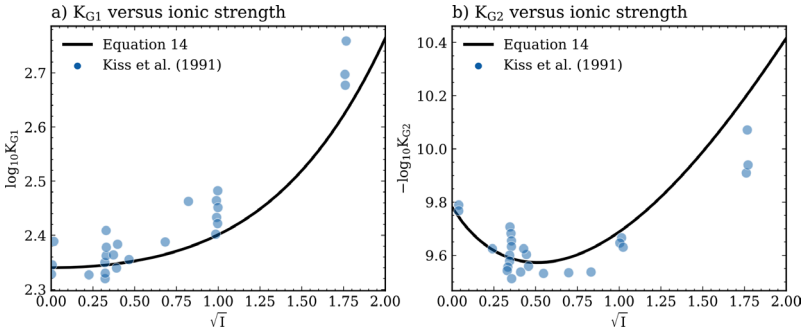

Fig. 3—Effect of ionic strength on the equilibrium constants for Reactions (a) G1 and (b) G2 in Table 3. The theoretical value was calculated using Eq. 14 and compared to the experimental values reported in Kiss et al. (1991).

No.	Reaction	z^*	C	D	E
G1	$GlyH + H^+ \Longleftrightarrow GlyH_2^+$	0	0.046	0	0.015
G2	$GlyH \Longleftrightarrow Gly^- + H^+$	-2	-0.316	0	0.008

Table 4—Parameters for Eq. 15 obtained by De Stefano et al. (2000) from fitting their experimental *K* values at ionic strengths up to 5.6 M.

The isoelectric point (p*I*) of glycine is defined as the arithmetic mean of the equilibrium constants of Reactions G1 and G2 in **Table 3**. The overall charge of glycine in solution depends on glycine's p*I* and the solution pH. For instance, glycine's overall charge is negative when its p*I* is greater than the solution pH. **Fig. 4** shows the impact of temperature (Eq. 13) and salinity (Eq. 14) on glycine's isoelectric point. The figure indicates that glycine's p*I* is lowest at low-salinity and high-temperature conditions, which means a higher concentration of glycine anion in solution.

The injection brine composition also affects glycine speciation because of the formation of aqueous complexes between glycine zwitterion and anion with Na^+, Ca^{2+}, and Mg^{2+} present in the aqueous phase. The carboxylic group of glycine interacts strongly with Ca^{2+} and

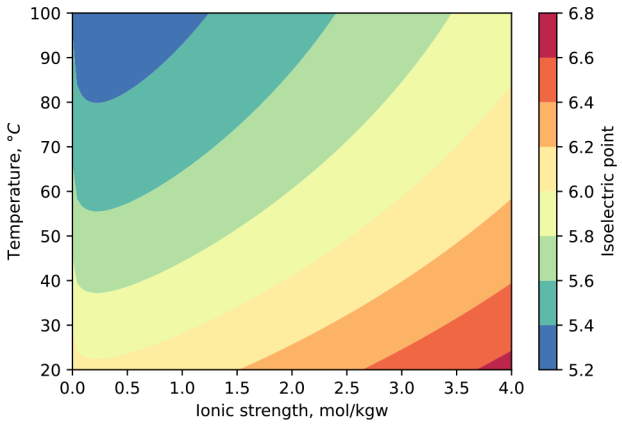

Fig. 4—Effect of temperature and ionic strength on glycine's p*I* calculated from the arithmetic average of the equilibrium constants of Reactions G1 and G2 in Table 3 adjusted using Eqs. 13 and 14.

Mg^{2+}, and weakly with Na^{+}. In this research, we considered the aqueous complexation reactions proposed by De Stefano et al. (2000) between glycine anion and Na^{+}, Ca^{2+}, and Mg^{2+} as shown in Reactions G3 to G7 in **Table 3**.

Glycine's Surface Complexation Reactions. Modeling the adsorption of glycine on the carbonate surface requires specifying the corresponding surface complexation reaction. It is known that glycine's carboxylic group can coordinate with divalent ions (Remko and Rode 2006). In particular, glycine anion strongly interacts with Ca^{2+} (De Stefano et al. 2000). Hence, we propose the following surface complexation reaction:

$$>CaOH_2^+ + Gly^- \Longleftrightarrow > CaGly + H_2O, \quad (15)$$

based on the analogous aqueous complexation reaction between glycine and calcium (Reaction G4 in **Table 3**). This approach has been followed by many researchers where surface complexation reactions and their equilibrium constants have been proposed based on the analogous aqueous complexation reaction [e.g., Van Cappellen et al. (1993), Pokrovsky et al. (1999), and Brady et al. (2012)].

Wettability Alteration Model. It is well-known that carbonate rocks become oil-wet because of the adsorption of organic components present in the crude oil (Kovscek et al. 1993). In the SCM, the acidic and basic components are represented by $-COO^-$ and $-NH_2^+$, respectively. The negatively charged acidic components, mainly naphthenic acids, have a strong affinity for the positively charged carbonate surfaces (Thomas et al. 1993; Sørgård and Seland 2020) as given by $>CaOH_2^+$-COO^-. The basic components, like pyridinic nitrogen bases, also affect the surface charge of the oil-brine interface and can interact with the negatively charged surface species to form $>CO_3^-$-NH_2^+ (Bonto et al. 2019).

In this research, we consider that the acidic components, $-COO^-$, dominate the interaction between crude oil and the carbonate surface, as concluded in Eftekhari et al. (2017). The wetting state of the rock surface is then determined by amount of acidic material from the crude oil that is adsorbed on to the rock surface **(Fig. 5)** as given by the following surface complexation reaction:

$$>CaOH_2^+ + -COO^- \Longleftrightarrow >CaOH_2^+ - COO^-. \quad (16)$$

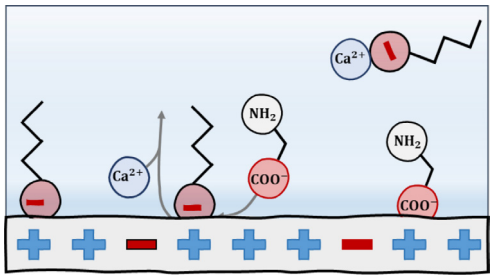

Fig. 5—Schematic illustration of the mechanism of wettability alteration by glycine anion and calcium ion. Magnesium ion can substitute the role of calcium ion.

The equilibrium constant ($\log_{10}K$) of the reaction in Eq. 16 has been mostly determined from matching oil displacement experiments. Qiao et al. (2016) reported a value of 5.90 by reproducing the initial wetting state of the coreflooding experiments with Stevns Klint chalk cores at 120°C as reported in Fathi et al. (2011). Sharma and Mohanty (2018) reported a value of 0.40 from matching the coreflooding experiments of Yousef et al. (2011) and Austad et al. (2015). However, they also considered the adsorption of acidic material on to the positive surface sites $>CO_3Mg^+$ and $>CO_3Ca^+$ with the same equilibrium constants. Chandrasekhar et al. (2018) used a simplified version of the SCM proposed by Sharma and Mohanty (2018) to match the coreflooding experiments using limestone reservoir cores reported in Chandrasekhar and Mohanty (2013). Eftekhari et al. (2017) defined $\log K_{S8} = -1.51$ and the enthalpy of reaction, $\Delta H_r = 4.96$ kJ·mol^{-1}, based on the analogous aqueous phase reaction. In this research, we considered the equilibrium constant and enthalpy of reaction values reported by Eftekhari et al. (2017) for reaction S8 in **Table 5.**

No.	Reaction			$\log_{10}K$ (25 °C)	ΔH_R (kJ/mol)
	Aqueous speciation				
O1	$-COO^- + H^+$	$\Longleftrightarrow$	$-COOH$	–4.80	0.00
	Aqueous complexation reactions				
O2	$-COOH + Ca^{2+}$	$\Longleftrightarrow$	$-COOCa^+ + H^+$	–3.40	1.17
O3	$-COOH + Mg^{2+}$	$\Longleftrightarrow$	$-COOMg^+ + H^+$	–3.40	-8.42
	Surface complexation reaction				
S8	$>CaOH_2^+ + -COO^-$	$\Longleftrightarrow$	$>CaOH_2^+\text{-}COO^- + H_2O$	–1.51	4.96

Table 5—Carboxylic acid's aqueous and surface reactions. The equilibrium constants and enthalpies of reaction for Reactions O1 to O3 are from Bonto et al. (2019). The equilibrium constant and the enthalpy of reaction for Reaction S8 are from Eftekhari et al. (2017).

The carboxylic acids, $-COO^-$, can also be protonated and form complexes with Ca^{2+} and Mg^{2+} (Bonto et al. 2019) described by Reactions O1 to O3 in **Table 5**. These chemical reactions follow the wettability alteration mechanism proposed in Zhang et al. (2007), where divalent ions SO_4^{2-}, Ca^{2+}, and Mg^{2+} work together to remove the carboxylic acids adsorbed from the rock surface. Furthermore, SO_4^{2-} adsorbs on to the rock surface (Reaction S2 in **Table 1**), removing the $-COO^-$ from $>CaOH_2^+$ sites. Glycine anion removes carboxylic acids in the same manner by reacting with $>CaOH_2^+$ (Reaction S7 in **Table 3**). At the same time, Ca^{2+} and Mg^{2+} aid the wettability modifiers by decreasing the activity of carboxylic acids (Reactions O2 and O3 in **Table 5**).

Finally, the amount of carboxylic acid in the system is determined by considering that the molar density of carboxylic acids, N_{-COO^-}, can be estimated from the crude oil total acid number, TAN in mg of KOH/g of oil, as proposed in Erzuah et al. (2019):

$$N_{-COOH} = \frac{TAN}{1000 a_{oil} MW_{KOH}}, \quad (17)$$

where a_{oil} is the specific surface area of oil ($m^2 \cdot g^{-1}$), and MW_{KOH} is the molecular weight of potassium hydroxide (56.1 $g \cdot mol^{-1}$). It was assumed that a_{oil} is equal to the rock's specific surface area.

Tuning Surface Complexation Reactions. The equilibrium constants of calcite's surface complexation reactions S1–S7 were tuned based on the ZP data for glycine solutions of single-component brines and FB and its dilutions reported in Lara Orozco et al. (2021). The function to be minimized is the root of the mean squared error (RMSE) between the experimental and calculated ZP given by

$$\text{RMSE} = \left[\frac{1}{N} \sum_{i=1}^{N} \left(\zeta_i^{\text{exp}} - \zeta_i^{\text{SCM}} \right)^2 \right]^{1/2}, \quad (18)$$

where ζ_i^{exp} and ζ_i^{SCM} are experimental and calculated ZP values, respectively. The basin-hopping algorithm (Wales and Doye 1997) from the SciPy library was used to find the global minimum of Eq. 18 with SLSQP as the local minimizer.

Model Verification

This section presents the verification of reactions of the SCM in PHREEQC using the calculated and experimental ZP values reported in Tetteh et al. (2020). We also verified the glycine aqueous reactions G1–G7 in **Table 2** and the effect of ionic strength estimated from Eq. 14 by comparing the calculated and measured pH of FB, SW, and LSW as a function of glycine concentration.

ZP of Indiana Limestone. Tetteh et al. (2020) measured the ZP of Indiana limestone by the electrophoretic mobility method at 25 and 40°C. **Table 6** shows the brine compositions investigated. They modified the SCM proposed by Brady et al. (2012) to fit their experimental results. The resulting SCM was further tested with the ZP data reported by Ding and Rahman (2018). We verified the implementation of the SCM in PHREEQC by reproducing the ZP calculated by Tetteh et al. (2020), as shown in **Fig. 6a.** We also compared the ZP calculated by the SCM with the experimental ZP reported in Tetteh et al. (2020) in **Fig. 6b**. The results show that the model overpredicted the ZP with formation water salinity (FWS in **Table 6**). This can be justified by increased nonidealities occurring in brines with high ionic strengths as discussed later in the FB and its Dilutions section. The SCM proposed by Tetteh et al. (2020) also overestimated the ZP of Na_2SO_4 brine and even predicted an opposite sign for the ZP of $CaCl_2$. The Verification of Tuned SCM section compares the predictions by the SMC in this research with the experimental ZP for Indiana limestone (Tetteh et al. 2020) along with the ZP data for natural calcite and limestone outcrops (Erzuah et al. 2019; Ding and Rahman 2018; Alroudhan et al. 2016).

	Ion Concentrations (mg/L)							
Brine	Ca^{2+}	Mg^{2+}	Na^+	K^+	Cl^-	SO_4^{2-}	I (mol/kgw)	TDS (ppm)
FWS	11 000	2800	48 000	500	101 913	260	3.27	164,473
SWS	2200	560	9600	100	20 383	52	0.65	32,895
LSW	134	34	585	6	1243	3	0.04	2,006

Table 6—Ionic compositions of the brines used in the ZP measurements of Indiana limestone reported in Tetteh et al. (2020). I = ionic strength; TDS = total dissolved solids.

Ion Concentrations (mg/L)								
Brine	Ca^{2+}	Mg^{2+}	Na^{+}	K^{+}	Cl^{-}	SO_4^{2-}	*I* (mol/kgw)	TDS (ppm)
NaCl	0	0	920	0	1418	0	0.04	2,338
KCl	0	0	0	1564	1418	0	0.04	2,982
$CaCl_2$	534	0	0	0	945	0	0.04	1,480
$MgCl_2$	0	324	0	0	945	0	0.04	1,269
Na_2SO_4	0	0	613	0	0	1 281	0.04	1,894

FWS, Formation Water Salinity;LSW, Low Salinity Water;SWS, Seawater Salinity.

Table 6 (continued)—Ionic compositions of the brines used in the ZP measurements of Indiana limestone reported in Tetteh et al. (2020). *I* = ionic strength; TDS = total dissolved solids.

Effect of Glycine on Brine pH. The addition of glycine to brines decreases the pH as given by Eq. 11. Since the speciation of glycine is affected by the brine composition and salinity, the solution pH as a function of glycine concentration will have different slopes for different brines. We verified glycine's aqueous reactions G1 to G4 shown in **Table 3** by calculating the pH of FB, SW, and LSW as a function of glycine's total concentration. The calculated pH is then compared with the values measured at glycine concentrations of 1, 3, and 5 wt% (Lara Orozco et al. 2021). The results shown in **Fig. 7** indicate a reasonable match between the experimental and calculated pH values even for FB, which has very high salinity.

Results and Discussion

This section shows the results from tuning the equilibrium constants of the surface complexation reactions S1 to S6 using the ZP data reported in Lara Orozco et al. (2021). Then, the SCM was used to estimate the concentrations of adsorbed carboxylic acids to qualitatively compare with the contact angle and spontaneous imbibition experiments reported in Lara Orozco et al. (2020). Finally, a sensitivity analysis of ZP and concentration of adsorbed carboxylic acids as a function of temperature and glycine concentration are shown, and their relationship with the wettability of carbonate rocks is discussed.

Tuned *K* Values of Surface Complexation Reactions. Two sets of the *K* values were obtained from matching the ZP data for synthetic calcite in glycine solutions prepared with single-component brines, and FB and its dilutions, as reported in Lara Orozco et al. (2021). The *K* values of Reactions S1 to S6 in **Table 1** were first tuned to match the ZP of brines without glycine. Then, the *K* value of Reaction S7 in **Table 3** was tuned to match the measured ZP of calcite in glycine solutions. The tuned SCM was compared with the SCMs proposed in Heberling et al. (2011) and Song et al. (2017) and several experimental ZP reported in the literature for synthetic calcite, natural calcite, and limestone outcrops.

Single-Component Brines. The optimization of the *K* values was first done using the single-component brines from **Table 7** and then the glycine solutions prepared with $CaCl_2$, $MgCl_2$, Na_2SO_4, and NaCl. In total, 25 ZP experimental points were used to tune the surface complexation reactions S1–S7. **Table 8** shows the initial and tuned equilibrium constants. The tuned values for Reactions S1–S6 using single-component brines are similar to the values in the literature **(Table 9).**

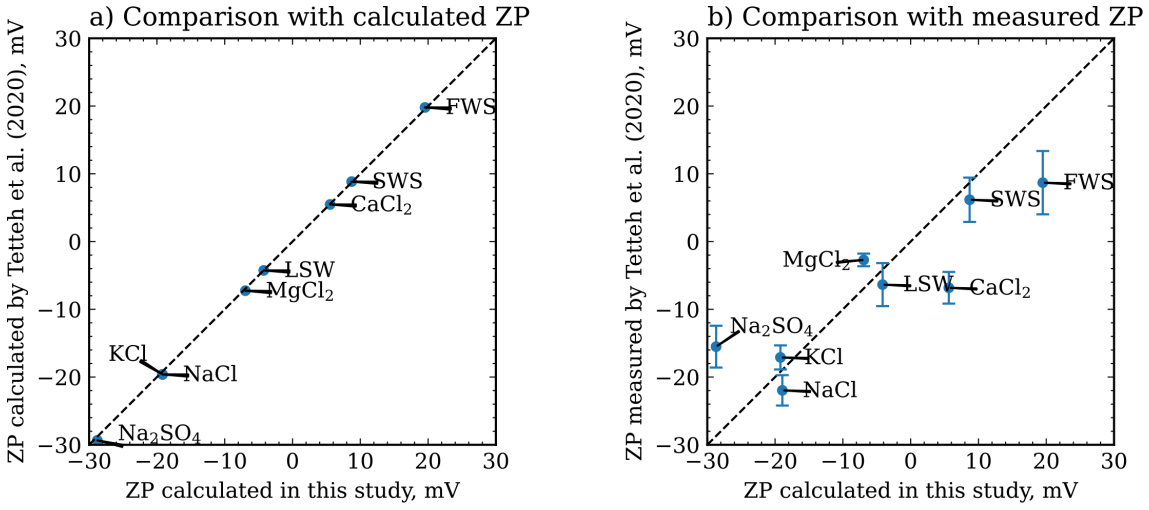

Fig. 6—Comparison between the ZPs at 25°C calculated in this research and the (a) calculated and (b) experimental values reported by Tetteh et al. (2020). The brine compositions are listed in Table 6. The surface complexation reactions considered were S1 to S6 using the equilibrium constants from Tetteh et al. (2020). The values for the site density and the specific surface area were 4.95 sites/nm^2 and 1 m^2/g, respectively.

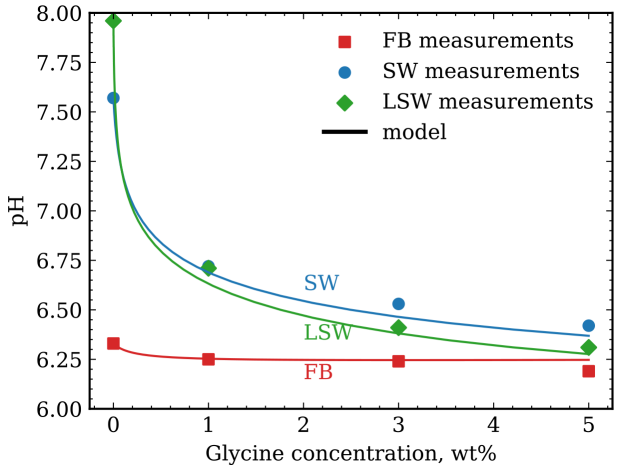

Fig. 7—Comparison between the measured and calculated pH for FB, SW, and LSW as a function of glycine concentration at 25°C and 1 atm reported in Lara Orozco et al. (2021). The ionic compositions of FB, SW, and LSW are in Table 10.

	Composition (mg/L)						
Brine	Na^+	Ca^{2+}	Mg^{2+}	Cl^-	SO_4^{2-}	HCO_3^-	Ionic Strength (mol/kgw)
25%-$CaCl_2$	671.77	36.87	0.00	1101.18	0.00	0.00	0.05
50%-$CaCl_2$	163.44	239.01	0.00	674.90	0.00	0.00	0.05
75%-$CaCl_2$	12.55	479.11	0.00	866.96	0.00	12.55	0.05
$CaCl_2$	766.32	0.00	0.00	0.00	1601.00	0.00	0.05
25%-$MgCl_2$	623.89	0.00	27.98	1043.75	0.00	0.00	0.05
50%-$MgCl_2$	131.34	0.00	156.28	658.39	0.00	0.00	0.05
75%-$MgCl_2$	9.60	0.00	293.71	871.51	0.00	0.00	0.05
$MgCl_2$	0.00	0.00	405.16	1181.76	0.00	0.00	0.05
25%-Na_2SO_4	764.15	0.00	0.00	1135.26	58.47	0.00	0.05
50%-Na_2SO_4	459.17	0.00	0.00	351.66	482.89	0.00	0.05
75%-Na_2SO_4	554.75	0.00	0.00	0	1117.23	0.00	0.05
Na_2SO_4	766.32	0.00	0.00	0	1601.00	0.00	0.05
NaCl	1149.49	0.00	0.00	1772.65	0.00	0.00	0.05

Table 7—Ionic compositions of single-component brines used in the ZP measurements of synthetic calcite reported in Lara Orozco et al. (2021).

				$\log_{10}K$ (25°C)		
No.	Surface Complexation Reaction			Initial	Tuned to Single-Component Brines	Tuned to FB and Its Dilutions
S1	$>CaOH_2^+$	$\Longleftrightarrow$	$>CaOH + H^+$	-11.85	-11.95	-10.24
S2	$>CaOH_2^+ + SO_4^-$	$\Longleftrightarrow$	$>CaSO_4^- + H_2O$	2.10	2.00	3.60
S3	$>CaOH_2^+ + CO_3^{2-}$	$\Longleftrightarrow$	$>CaCO_3^- + H_2O$	4.28	3.80	6.04
S4	$>CO_3^- + H^+$	$\Longleftrightarrow$	$>CO_3H$	5.10	5.08	6.54
S5	$>CO_3^- + Ca^{2+}$	$\Longleftrightarrow$	$>CO_3Ca^+$	2.50	2.08	1.80
S6	$>CO_3^- + Mg^{2+}$	$\Longleftrightarrow$	$>CO_3Mg^+$	2.50	1.90	1.27
S7	$>CaOH_2^+ + Gly^-$	$\Longleftrightarrow$	$>CaGly + H_2O$	1.40	1.93	1.22

Table 8—Tuned equilibrium constants of surface complexation reactions based on the ZP measurements with glycine solutions reported in Lara Orozco et al. (2020). The initial equilibrium constants are from Brady et al. (2012).

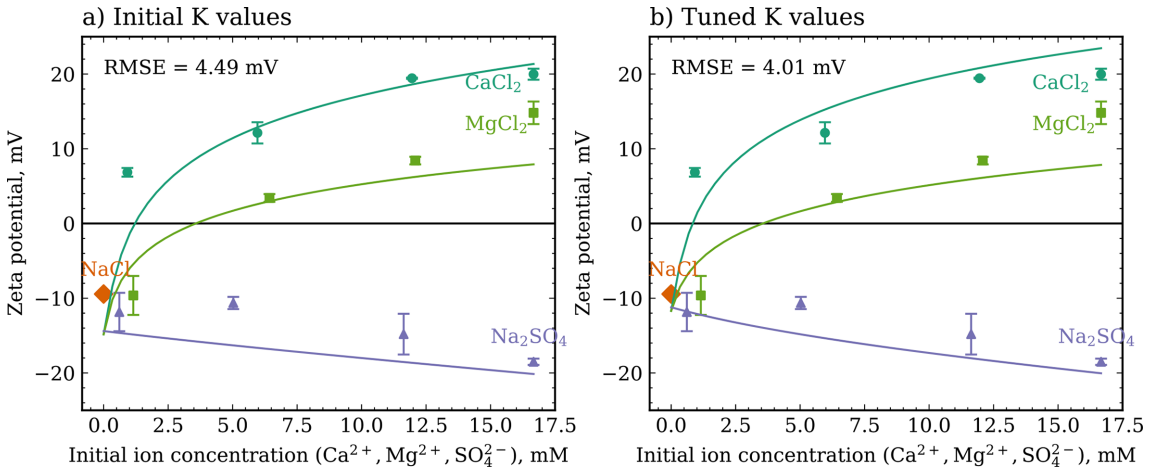

Fig. 8—Comparison between the ZP calculated by the SCM and the experimental ZP of single-component brines reported in Lara Orozco et al. (2020). The initial and tuned equilibrium constants are in Table 8. RMSE is the root mean square (RMS) error defined in Eq. 18.

No.	Surface Species	Reference: Van Cappellen et al. (1993)	Pokrovsky and Schott (2002)	Brady et al. (2012)	Tetteh et al. (2020)	Sanaei et al. (2019)	Hiorth et al. (2010)	Qiao et al. (2016)
S1	>CaOH	-12.2	-11.85	-11.85	-11.85	-11.6	-12.90	-11.80
S2	$>CaSO_4^-$	-	-	2.10	2.10	2.1	2.10	-2.10
S3	$>CaCO_3^-$	3.35	5.25	4.53	4.28	4.53	3.32	6.00
S4	$>CO_3H$	4.90	5.10	5.10	5.10	4.6	4.90	5.10
S5	$>CO_3Ca^+$	2.10	3.40	2.50	0.70	2	1.74	2.50
S6	$>CO_3Mg^+$	-	-	2.50	0.70	2.5	1.73	2.50

Table 9—Equilibrium constants of surface complexation reactions reported in the literature.

Figs. 8 and 9 show the comparison between the experimental and the calculated ZP using the initial and tuned equilibrium. The ZP values calculated by the SCM using the initial *K* values were in excellent agreement with the experimental data **(Fig. 8a)**. However, **Fig. 9a** shows that with the initial *K* values the SCM overpredicted the ZP of NaCl and Na_2SO_4 glycine solutions. The matching of the experimental ZP values was improved significantly as shown in **Fig. 9b**, mainly because of the increase of the *K* value of glycine's surface complexation reaction from $\log_{10} K$=1.40 to $\log_{10} K$=1.93.

FB and its Dilutions. The optimization of the *K* values was done separately using the glycine solutions with FB and its dilutions because no satisfactory solution was found when using both FB and single-component brines. The *K* values were optimized to match the

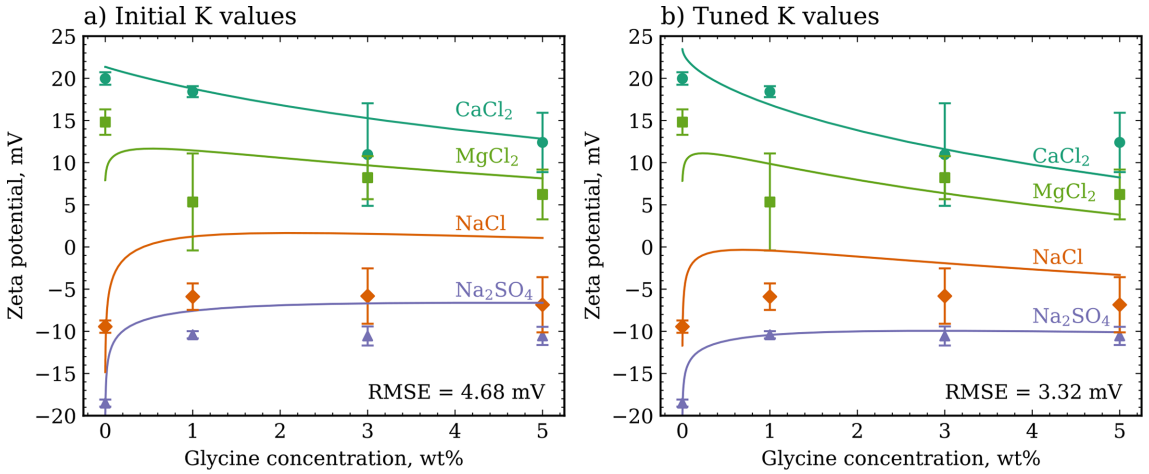

Fig. 9—Comparison between ZP calculated by the SCM and the experimental ZP of glycine solutions with single-component brines reported in Lara Orozco et al. (2020). The initial and tuned equilibrium constants are in Table 8. RMSE is the RMS error defined in Eq. 18.

experimental results as previously. However, in this case, the K values were constrained to change up to two orders of magnitude during the optimization process to not significantly deviate from the K values published in the literature.

Fig. 10 shows the comparison between the calculated and experimental ZP values for FB and its dilutions using the initial and tuned K values. The SCM with the initial K values significantly overpredicted the experimental results. Similar results were obtained using the equilibrium constants tuned using the single-component brine results because these are not very different from the initial K values (**Table 8**). As expected, the tuned SCM significantly improved the matching as shown in **Fig. 10b**. However, the trend of increasing ZP for 100 dFB when adding 1 wt% glycine was not reproduced by the model. The SCM predicted a minimal impact of glycine on the ZP as observed with the experimental results for FB and 2 dFB. The tuned equilibrium constant for Reaction S7 for glycine adsorption ($\log_{10} K$=1.22) was lower than the initial value ($\log_{10} K$=1.40).

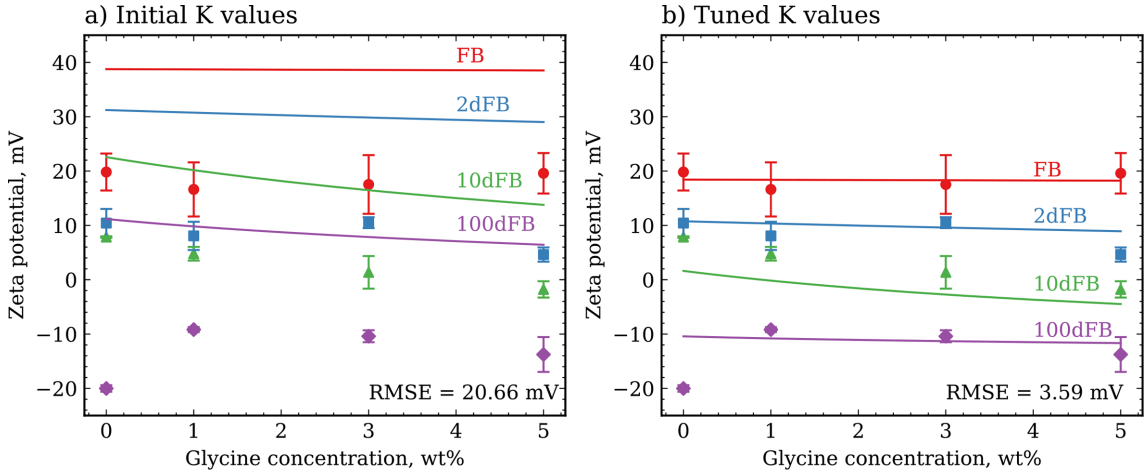

Fig. 10—Comparison between ZP calculated by the SCM and the experimental ZP of glycine solutions with FB and its dilutions reported in Lara Orozco et al. (2020). The initial and tuned equilibrium constants are in Table 8. RMSE is the RMS error defined in Eq. 18.

After tuning the SCM, two K values were obtained for glycine surface complexation, $\log_{10} K$=1.22 and $\log_{10} K$=1.93. The tuned K value obtained from matching the results with single-component brines, $\log_{10} K$=1.93, was used in the rest of this work for the following reasons. First, the measurements with single-component brines considered a wider range of brine compositions, and more experimental points were available to tune the SCM. Second, single-component brines are closer to ideal solutions with ionic strength of 0.05 M where, in comparison, FB and 10 dFB are highly nonideal brines with ionic strengths of 6.37 and 3.32 M, respectively. Finally, the estimated equilibrium constant for Reaction S7 is more reliable because both the experimental and the calculated ZP values for single-component brines were more sensitive to the addition of glycine in comparison to the measurements using FB and its dilutions.

The overprediction of the ZP values for the FB and its dilutions could be caused by the assumptions in the SCM. For instance, Eq. 7 used to estimate the slip plane distance was derived for solutions with ionic strengths in the range of 10^{-4} to 1 M (Heberling et al. 2011). Also, the activity models for ions in the aqueous phase described in section Aqueous Chemistry are valid for ionic strengths up to 2 M in dominantly chloride solutions (Parkhurst 1990; Appelo and Postma 2005). Hence, Eq. 8 might overpredict the activity of divalent cations that would result in high concentrations of the positively charged surface species, $>CO_3Ca^+$ and $>CO_3Mg^+$. Activity coefficients could be calculated more accurately for high-salinity brines using Pitzer correlations (Appelo 2015); however, their inclusion in the SCM is out of the scope of this research.

Verification of Tuned SCM. This section is to demonstrate the range of applicability of the tuned SCM proposed in this study and to compare it with the SCMs proposed by Heberling et al. (2011) and Song et al. (2017). Heberling et al. (2011) proposed a basic Stern tune to their ZP measurements of synthetic calcite measured by the electrophoretic mobility and stream potential methods. Their SCM consists of a Stern layer with constant capacitance layer and a diffuse layer described by the Gouy-Chapman theory (Eq. 4). The SCM proposed by Song et al. (2017) is based on the Heberling et al. model but considers a diffuse layer model. The Song et al. SCM was tuned using

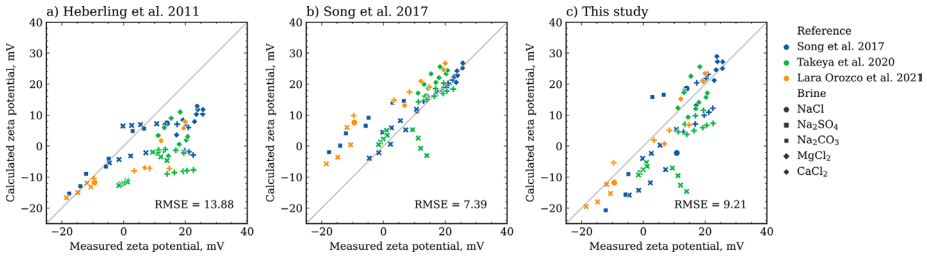

Fig. 11—Comparison between the experimental ZPs of synthetic calcite reported in the literature and the predictions using (a) the Heberling et al. model, (b)the Song et al. model, and (c) the SCM in this study tuned using single-component brines. The root mean square error (RSME) is defined in Eq. 18. References (Heberling et al. 2011; Song et al. 2017; Takeya et al. 2020; Lara Orozco et al. 2021).

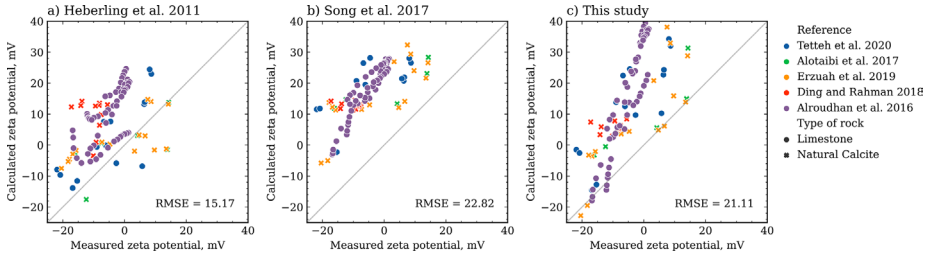

Fig. 12—Comparison between the experimental ZPs of natural calcite and limestone outcrops reported in the literature and the predictions using (a) the Heberling et al. model, (b) the Song et al. model, and (c) the SCM in this study tuned using single-component brines. The root mean square error (RSME) is defined in Eq. 18. References (Alroudhan et al. 2016; Alotaibi and Yousef 2016; Ding and Rahman 2018; Erzuah et al. 2019; Tetteh et al. 2020).

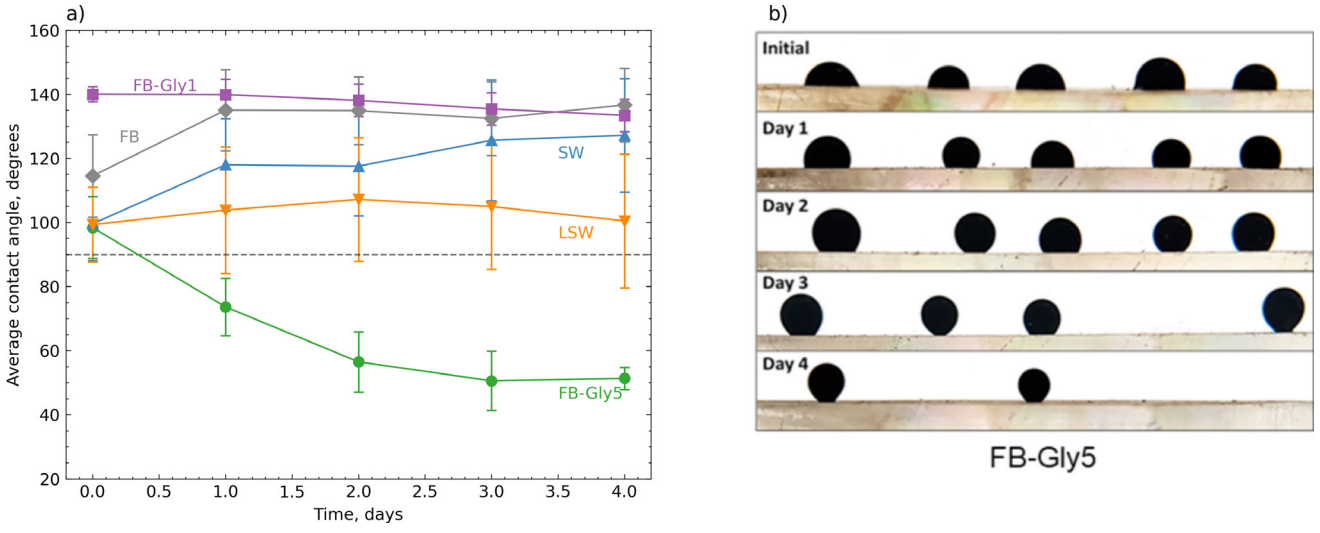

Fig. 13—(a) Contact angle measurements at 95°C as a function of time. The compositions of the brines (FB, SW, and LSW) are mentioned in Table 10. The labels FB-Gly1 and FB-Gly5 indicate that 1 and 5 wt% of glycine concentration in FB, respectively. (b) Visualization of oil droplets contact angle changing with time for FB-Gly5.

the ZP of synthetic calcite particles measured in single-component brines prepared with Na_2CO_3 , Na_2SO_4 , NaCl, $MgCl_2$, and $CaCl_2$ equilibrated using CO_2 partial pressures of $10^{-3.4}$ and 1 atm.

Fig. 11 shows the comparison of the measured and calculated ZP values using the SCMs from Heberling et al. (2011) and Song et al. (2017) along with the SCM obtained from matching single-component brines in the Single-Component Brines section. The Heberling et al. model does not include the adsorption of magnesium ions; hence, we included this reaction with the same *K* value proposed for the adsorption of calcium ions. The Heberling et al. model only satisfactorily matched the ZP of Na_2SO_4 brines from Lara Orozco et al. (2021) and Na_2CO_3 from Song et al. (2017), while underestimating the ZP reported by Takeya et al. (2020). The Song et al. model reasonably matched the ZP of Takeya et al. (2020) and there is a systematical overprediction of the ZP from Lara Orozco et al. (2021). Similarly, the SCM from this study systematically underpredicted the ZP from Song et al. (2017) and Takeya et al. (2020). The comparison shows the difficulty of predicting the ZP reported by other researchers. The Heberling et al. model yielded the highest error because none of the experimental ZP used in the comparison were used to tune the SCM.

Fig. 12 compares the calculated and measured ZP for natural calcite and limestone outcrops. It shows the application of the SCMs to predict the ZP of carbonates with different mineralogy. The three models overpredicted the experimental ZP values; however, the Heberling et al. model yielded the lowest error. The overprediction of the ZP values agrees with the SCM proposed in Tetteh et al. (2020) for Indiana limestone where the *K* values for the adsorption of calcium and magnesium (Reactions S5 and S6 in **Table 1**) had to be from 2.5 to 0.7 to improve the matching of the experimental results. The ZP of natural carbonates having a more negative ZP than synthetic calcite has been attributed to the presence of inorganic and organic impurities (Al Mahrouqi et al. 2017).

Effect of Glycine Concentration and Temperature on ZP and Adsorbed Carboxylic Acids. For this section, the reactions of carboxylic acids in **Table 5** were included in the tuned SCM. The calculated concentrations of adsorbed carboxylic acids were qualitatively compared with the experimental data with glycine solutions reported in Lara Orozco et al. (2020) using FB, SW, and LSW, as listed in **Table 10.** For convenience, the relevant results of the contact angle measurements and spontaneous imbibition experiments reported in Lara Orozco et al. (2020) are summarized below.

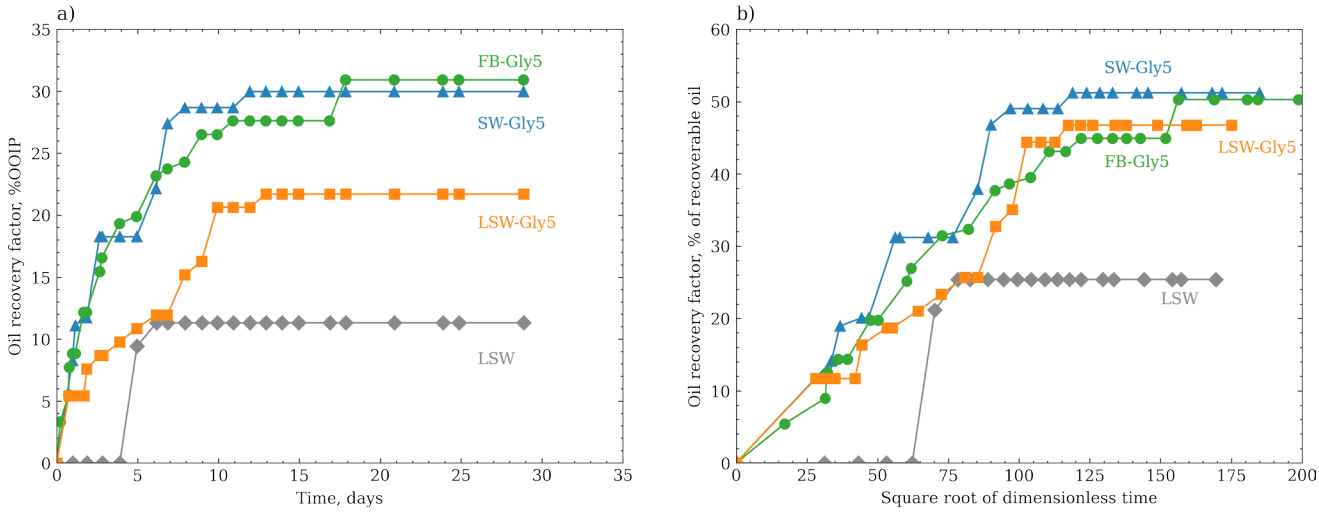

Fig. 14—Spontaneous imbibition experimental results with Indiana limestone at 95 °C from Lara Orozco et al. (2020). (a) Oil recovery is expressed in the percentage of oil originally in place versus time. (b) Oil recovery is expressed as the percentage of recoverable oil versus the square root of dimensionless time.

Ion Concentrations (mg/L)

Brine	Ca^{2+}	Mg^{2+}	Na^{+}	Cl^{-}	SO_4^{2-}	HCO_3^{-}	*I* (mol/kgw)	TDS (ppm)
FB	19 080	2561	70 991	150 165	588	186	6.37	243,571
SW	2880	536	22 928	40 500	1765	366	1.36	68,975
LSW	288	54	2 293	4050	177	37	0.13	6,898

Table 10—Ionic composition of the brines used for the contact angle measurements and spontaneous imbibition experiments with glycine solutions reported in Lara Orozco et al. (2020). *I* = ionic strength; TDS = total dissolved solids.

The contact angle measurements were conducted at 95°C using natural calcite (Iceland spar). The calcite pieces were previously aged at 95°C using crude oil with a total acid number, TAN, of 0.13 mg KOH/g. Five to six oil droplets were placed on the calcite piece and the average contact angle was reported along with its standard deviation. **Fig. 13** shows the change of the average contact angle with time. The reference case is FB, which had a final contact angle of 130°. The solution of 5 wt% glycine in FB (FB-Gly5) yielded the lowest final contact angle of 50° (after 4 days). Even lower contact angle values could have been achieved, but the oil droplets detached from the calcite surface **(Fig. 13b)**. The solution of 1 wt% glycine in FB had a final contact angle that was similar to the FB case. However, the initial contact angle, 140°, was higher than the other solutions and a decreasing trend was observed to a final contact angle of 134° (after 4 days). The final contact angle for SW was also close to FB, 129°, while the final contact angle for LSW was 102°. This was consistent with the low-salinity effect reported in the literature (Hao et al. 2019), but it did not yield a strongly water-wet surface as was the case with FB-Gly5.

The spontaneous imbibition experiments were also conducted at 95°C with Indiana limestone cores of 2.54 cm in diameter and 1.27 cm in length. The experiments used the solutions of 5 wt% glycine in FB, SW, and LSW, which are labeled as FB-Gly5, SW-Gly5,

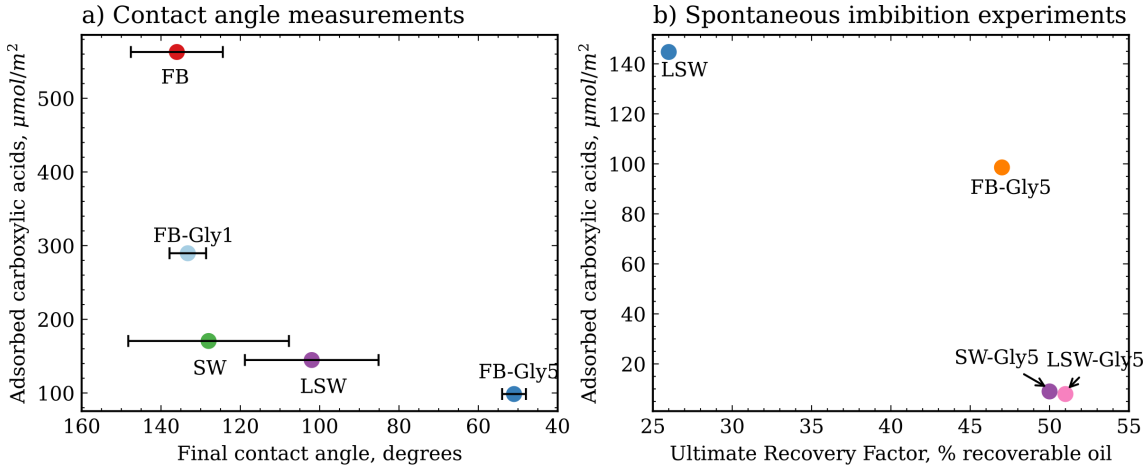

Fig. 15—The concentration of adsorbed carboxylic acids calculated by the SCM and (a) the final contact angles from Fig. 13 and (b) the ultimate recovery factor in terms of recoverable oil from Fig. 14. The results from the SCM are at 95°C and in equilibrium with calcite and atmospheric CO_2.

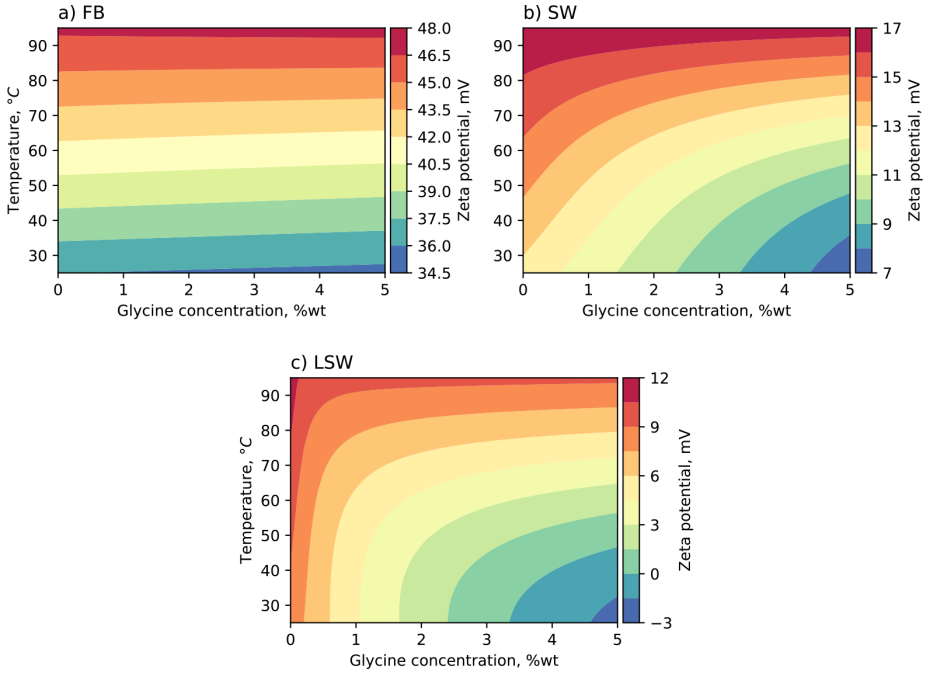

Fig. 16—Impact of temperature and glycine concentration on the ZP of calcite in (a) FB, (b) SW, and (c) LSW, calculated using the tuned SCM at 95°C and in equilibrium with calcite and atmospheric CO_2. The brine compositions are mentioned in Table 10.

and LSW-Gly5, respectively. LSW was selected for the reference case because it was expected to recover more oil than FB and SW. **Fig. 14** shows the oil recovery history (Lara Orozco et al. 2020). The ultimate oil recoveries for FB-Gly5 and SW-Gly5 were similar to each other—30.9 and 30.0% oil originally in place, respectively. The ultimate oil recovery was 11.3% for LSW and 27.7% for LSW-Gly5; in other words, this direct comparison with/without glycine clarified the oil recovery enhanced by the addition of glycine to LSW. Since the cores inevitably had slightly different petrophysical properties and initial oil saturations, the results were plotted in terms of the percentage of recoverable oil with respect to the square root of dimensionless time. The results shown in **Fig. 14b** suggest that the three glycine solutions yield similar oil recoveries and that there was an evident oil recovery enhancement in comparison to LSW.

Fig. 15 shows the comparison between the concentration of adsorbed carboxylic acids calculated by the SCM and the results from the contact angle measurements and the spontaneous imbibition experiments. The SCM correctly predicts the order of the wetting state for

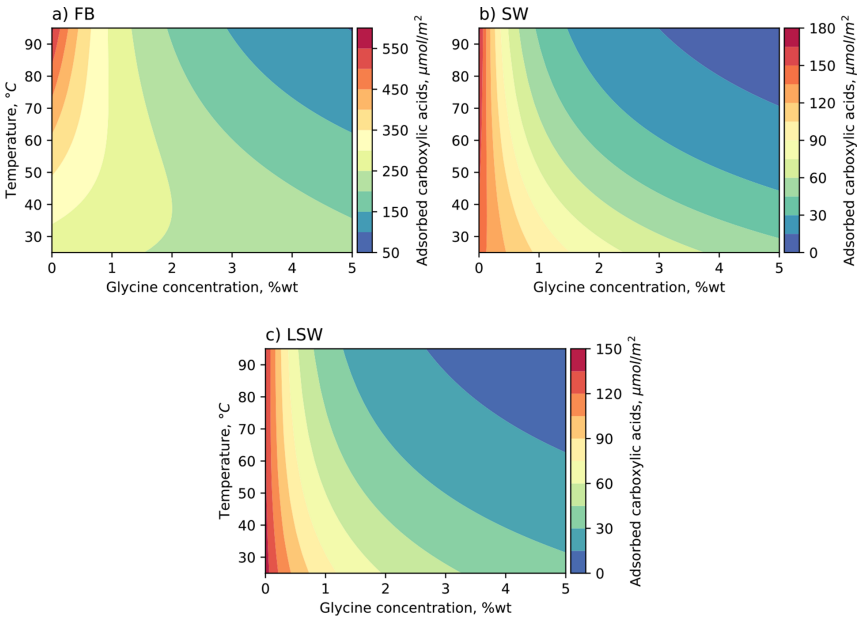

Fig. 17—Impact of temperature and glycine concentration on the concentration of adsorbed carboxylic acids for (a) FB, (b) SW, and (c) LSW, calculated using the tuned SCM at 95°C and in equilibrium with calcite and atmospheric CO_2. The brine compositions are mentioned in Table 10.

FB, FB-Gly5, SW, and LSW brines observed in the contact angle measurements **(Fig. 13a)**. However, the SCM indicates that the wetting state of FB-Gly1, SW, and LSW is similar to FB-Gly5, while in the experiments the contact angles measured in FB-Gly1, SW, and LSW were closer to FB. For the spontaneous imbibition experiments, the SCM predicts the incremental oil recovery obtained by glycine solutions compared to LSW. The SCM, however, suggests that EOR should be higher for SW-Gly5 and LSW-Gly5 than FB-Gly5, while the results showed similar recovery factors for the three glycine solutions. In general, the SCM shows good agreement with the experimental results. The observed discrepancies can be explained by both the uncertainty on the experimental measurements and the limitations of the SCM for high-salinity brines, as previously explained in the Tuned *K* Values of Surface Complexation Reactions section, and the validity of the van't Hoff equation at high temperatures.

Effect of Glycine Concentration and Temperature on ZP and Adsorbed Carboxylic Acids. As explained in the Tuning Surface Complexation Reactions section, we modeled wettability alteration through the concentration of adsorbed carboxylic acids on the rock surface. However, the ZP of calcite has been directly or indirectly related to the wetting state of carbonate rocks (Brady et al. 2012; Korrani and Jerauld 2019; Bonto et al. 2020). In general, increasing oil recovery observed in coreflooding and spontaneous imbibition experiments have been related to more water-wetting conditions resulting from decreasing ZP values. It is insightful to show the differences in wetting state indicated by the ZP values and the calculated concentrations of adsorbed carboxylic acids as a function of temperature and glycine concentration for FB, SW, and LSW as discussed below.

Fig. 16 shows the ZP of calcite in FB, SW, and LSW predicted by the tuned SCM for different glycine concentrations and temperatures. **Fig. 16a** shows that the ZP of calcite in FB is insensitive to glycine concentration at any temperature, while the impact of glycine on calcite's ZP in SW and LSW is more significant at low temperatures. The decreasing ZP for SW and LSW without glycine correlates with the EOR observed in the corefloods and spontaneous imbibition results reported in the literature. However, the calculated ZP as a function of glycine concentration indicates that a more water-wetting state should be obtained at lower temperatures, which was not observed in the experiments with glycine by Lara Orozco et al. (2020).

Fig. 17 shows the concentrations of adsorbed carboxylic acids predicted by the tuned SCM for different glycine concentrations and temperatures. The results suggest that wettability alteration of carbonate rocks by glycine is more significant at high temperatures. Also, the trends predicted by the SCM were similar for FB, SW, and LSW. In general, the concentration of adsorbed carboxylic acids is a better indicator of wettability alteration by glycine solutions than the ZP.

Conclusions

We presented a surface complexation reaction of glycine and its adsorption on to calcite surfaces. Equilibrium constants were estimated from the published ZP data of calcite in glycine solutions. The aqueous and surface reactions of glycine were included in calcite's SCM to investigate the impact of glycine on the ZP of synthetic calcite particles. The impact of glycine on the wettability alteration of carbonate rocks was also investigated by considering the adsorption of carboxylic acids on to the calcite surface. The resulting model quantifies the impact of glycine on the wetting state of carbonate rocks as a function of temperature, salinity, and brine composition. The main conclusions of this research are as follows:

- SCMs have limitations regarding the prediction of high-salinity brines (i.e., FB in this research). The model overpredicted the ZP of calcite in FB and its dilutions. This can be explained by the overprediction of the activity of calcium and magnesium ions using the Truesdell and Jones activity model.
- The interaction between glycine and carbonate surface is affected by the concentration of glycine anion. Its concentration can be increased by decreasing glycine's p*I* and/or increasing solution pH equilibrated with calcite.
- Temperature is likely an important factor affecting glycine's performance as a wettability modifier. Increasing temperature significantly increases the second deprotonation constant of reaction G2 that results in a higher concentration of glycine anion. It was observed that the calculated desorption of carboxylic acid as a function of glycine concentration was significantly higher at 95°C than 25°C.
- The concentration of carboxylic acid adsorbed on the surface was found to be a direct indicator of carbonate rock's wettability. The change in the concentration of adsorbed carboxylic acid predicted by the SCM correlated well with the contact angle and spontaneous imbibition experiments with glycine solutions in contrast to the calculated ZP.
- Glycine performs for all three brines (FB, SW, and LSW) as a wettability modifier. At 95°C, the SCM indicates that 1 wt% glycine in FB would yield a similar amount of desorption of carboxylic acids to the use of SW or LSW.
- The proposed SCM can be used to investigate incremental oil recovery obtained by glycine addition to waterflooding in carbonate reservoirs. The ZP calculated by the SCM was in excellent agreement with the experimental values obtained using single-component brines. Also, the calculated concentrations of adsorbed carboxylic acids satisfactorily followed the trends observed in the contact angle measurements and spontaneous imbibition experiments.

Nomenclature

a_{oil} = oil specific surface area, $m^2 \cdot g^{-1}$
A = solid specific surface area, $m^2 \cdot g^{-1}$
C, D, E = empirical parameters for Eq. 15
d_s = slip plane, nm
e = elementary charge, 1.602×10^{-19} C
F = Faraday's constant, 96 485 $C \cdot mol^{-1}$
I = solution ionic strength, $mol \cdot dm^{-3}$
k_b = Boltzmann constant, J·K-1 1.381×10
K_{app} = apparent equilibrium constant
K = intrinsic equilibrium constant
m_{si} = molar concentration of surface species *i*, $mol \cdot L^{-1}$
MW_{KOH} = molecular weight of potassium hydroxide, 56.1 $g \cdot mol^{-1}$
N_A = Avogadro's number, 6.022×10^{23} mol^{-1}
R = universal gas constant, 8.314 $J \cdot mol^{-1} \cdot K^{-1}$
S = solid concentration, $g \cdot L^{-1}$
T = absolute temperature, K
T_r = reference absolute temperature, K

TAN = total acid number, mg of KOH/g of oil
z_{si} = electrical charge of surface species i
ε_0 = permittivity of free space, 8.854×10^{-12} C·V^{-1}·m^{-1}
ε_ω = relative permittivity of the solution, 78.5 for water at 25°C
ΔC_p^0 = standard partial molar heat capacity of reaction, J·K^{-1}·mol^{-1}
ΔH_R = enthalpy of reaction, J·mol^{-1}
Δz = net change of surface charge
σ = surface charge density, C·m^{-2}
ψ = surface potential, V
ζ = zeta potential, V

Acknowledgments

Ryosuke Okuno holds the Pioneer Corporation Faculty Fellowship in Petroleum Engineering at the University of Texas at Austin. Larry W. Lake holds the Shahid and Sharon Ullah Chair at the University of Texas at Austin.

References

Al Mahrouqi, D., Vinogradov, J., and Jackson, M. D. 2017. Zeta Potential of Artificial and Natural Calcite in Aqueous Solution. *Adv Colloid Interface Sci* **240**: 60–76. https://doi.org/10.1016/j.cis.2016.12.006.

Alotaibi, M. B. and Yousef, A. A. 2016. The Role of Individual and Combined Ions in Waterflooding Carbonate Reservoirs: Electrokinetic Study. *SPE Res Eval & Eng* **20** (1): 077–086. SPE-177983-PA. https://doi.org/10.2118/177983-PA.

Alroudhan, A., Vinogradov, J., and Jackson, M. D. 2016. Zeta Potential of Intact Natural Limestone: Impact of Potential-Determining Ions Ca, Mg and SO4. *Colloids and Surfaces A* **493**: 83–98. https://doi.org/10.1016/j.colsurfa.2015.11.068.

Appelo, C. A. J. 2015. Principles, Caveats and Improvements in Databases for Calculating Hydrogeochemical Reactions in Saline Waters from 0 to 200 °C and 1 to 1000 Atm. *Appl. Geochem.* **55**: 62–71. https://doi.org/10.1016/j.apgeochem.2014.11.007.

Appelo, C. A. J. and Postma, D. 2005. *Geochemistry, Groundwater and Pollution*, second edition. London, United Kingdom: CRC Press.

Austad, T., Shariatpanahi, S. F., Strand, S. et al. 2015. Low Salinity EOR Effects in Limestone Reservoir Cores Containing Anhydrite: A Discussion of the Chemical Mechanism. *Energy Fuels* **29** (11): 6903–6911. https://doi.org/10.1021/acs.energyfuels.5b01099.

Bonto, M., Eftekhari, A. A., and Nick, H. 2021. Analysis of the Temperature Impact on the Calcite Surface Reactivity in Modified Salinity Water Applications. Paper presented at the EAGE Improved Oil Recovery Symposium, Online Event, 19–22 April. https://doi.org/10.3997/2214-4609.202133082.

Bonto, M., Eftekhari, A. A., and Nick, H. M. 2019. An Overview of the Oil-Brine Interfacial Behavior and a New Surface Complexation Model. *Sci Rep* **9** (1): 1–16. https://doi.org/10.1038/s41598-019-42505-2.

Bonto, M., Eftekhari, A. A., and Nick, H. M. 2020. Wettability Indicator Parameter Based on the Thermodynamic Modeling of Chalk-Oil-Brine Systems. *Energy Fuels* **34** (7): 8018–8036. https://doi.org/10.1021/acs.energyfuels.0c00716.

Bordeaux-Rego, F., Mehrabi, M., Sanaei, A. et al. 2021. Improvements on Modelling Wettability Alteration by Engineered Water Injection: Surface Complexation at the Oil/Brine/Rock Contact. *Fuel* **284**: 118991. https://doi.org/10.1016/j.fuel.2020.118991.

Brady, P. V., Krumhansl, J. L., and Mariner, P. E. 2012. Surface Complexation Modeling for Improved Oil Recovery. Paper presented at the SPE Improved Oil Recovery Symposium, Tulsa, Oklahoma, USA, 14–18 April. SPE-153744-MS. https://doi.org/10.2118/153744-MS.

Chandrasekhar, S. and Mohanty, K. K. 2013. Wettability Alteration with Brine Composition in High Temperature Carbonate Reservoirs. Paper presented at the SPE Annual Technical Conference and Exhibition, New Orleans, Louisiana, USA, 30 September–2 October. SPE-166280-MS. https://doi.org/10.2118/166280-MS.

Chandrasekhar, S., Sharma, H., and Mohanty, K. K. 2018. Dependence of Wettability on Brine Composition in High Temperature Carbonate Rocks. *Fuel* **225**: 573–587. https://doi.org/10.1016/j.fuel.2018.03.176.

Christensen, J. J., Izatt, R. M., and Hansen, L. D. 1967. Thermodynamics of Proton Ionization in Dilute Aqueous Solution. VII. [UNK] H ° and [UNK] S ° Values for Proton Ionization from Carboxylic Acids at 25°. *J. Am. Chem. Soc.* **89** (2): 213–222. https://doi.org/10.1021/ja00978a005.

Clarke, R. G. F., Collins, C. M., Roberts, J. C. et al. 2005. Ionization Constants of Aqueous Amino Acids at Temperatures up to 250°C Using Hydrothermal PH Indicators and UV-Visible Spectroscopy: Glycine, α-Alanine, and Proline. *Geochim. Cosmochim. Acta* **69** (12): 3029–3043. https://doi.org/10.1016/j.gca.2004.11.028.

De Stefano, C., Foti, C., Gianguzza, A. et al. 2000. The Interaction of Amino Acids with the Major Constituents of Natural Waters at Different Ionic Strengths. *Mar Chem* **72** (1): 61–76. https://doi.org/10.1016/S0304-4203(00)00067-0.

Ding, H. and Rahman, S. R. 2018. Investigation of the Impact of Potential Determining Ions from Surface Complexation Modeling. *Energy Fuels* **32** (9): 9314–9321. https://doi.org/10.1021/acs.energyfuels.8b02131.

Dzombak, D. A. and Morel, F. M. 1990. *Surface Complexation Modeling: Hydrous Ferric Oxide*. Chichester, United Kingdom: John Wiley & Sons.

Eftekhari, A.A., Thomsen, K., Stenby, E.H. et al. 2017. Thermodynamic Analysis of Chalk–Brine–Oil Interactions. *Energy Fuels* **31**(11): 11773–11782. https://doi.org/10.1021/acs.energyfuels.7b02019.

Erzuah, S., Fjelde, I., and Omekeh, A. V. 2019. Wettability Estimation Using Surface-Complexation Simulations. *SPE Res Eval & Eng* **22** (2): 509–519. SPE-185767-PA. https://doi.org/10.2118/185767-PA.

Fathi, S. J., Austad, T., and Strand, S. 2011. Water-Based Enhanced Oil Recovery (EOR) by "Smart Water": Optimal Ionic Composition for EOR in Carbonates. *Energy Fuels* **25** (11): 5173–5179. https://doi.org/10.1021/ef201019k.

Gillespie, S. E., Oscarson, J. L., Izatt, R. M. et al. 1995. Thermodynamic Quantities for the Protonation of Amino Acid Amino Groups from 323.15 to 398.15 K. *J Solution Chem* **24** (12): 1219–1247. https://doi.org/10.1007/BF00972830.

Gupta, M. and Svendsen, H. F. 2013. Modeling Temperature Dependency of Ionization Constants of Amino Acids and Carboxylic AcidsModeling Temperature Dependency of Ionization Constants of Amino Acids and Carboxylic Acids. *J Phys Chem B* **117** (25): 7695–7709. https://doi.org/10.1021/jp402496u.

Hamborg, E. S., Niederer, J. P. M., and Versteeg, G. F. 2007. Dissociation Constants and Thermodynamic Properties of Amino Acids Used in CO 2 Absorption from (293 to 353) K. *J. Chem. Eng. Data* **52** (6): 2491–2502. https://doi.org/10.1021/je700275v.

Hao, J., Mohammadkhani, S., Shahverdi, H. et al. 2019. Mechanisms of Smart Waterflooding in Carbonate Oil Reservoirs - A Review. *J Pet Sci Eng* **179**: 276–291. https://doi.org/10.1016/j.petrol.2019.04.049.

Heberling, F., Trainor, T. P., Lützenkirchen, J. et al. 2011. Structure and Reactivity of the Calcite-Water Interface. *J Colloid Interface Sci* **354** (2): 843–857. https://doi.org/10.1016/j.jcis.2010.10.047.

Hiorth, A., Cathles, L. M., and Madland, M. V. 2010. The Impact of Pore Water Chemistry on Carbonate Surface Charge and Oil Wettability. *Transp Porous Med* **85** (1): 1–21. https://doi.org/10.1007/s11242-010-9543-6.

Izatt, R. M., Oscarson, J. L., Gillespie, S. E. et al. 1992. Effect of Temperature and Pressure on the Protonation of Glycine. *Biophys J* **61** (5): 1394–1401. https://doi.org/10.1016/S0006-3495(92)81945-8.

Karty, K. 2018. *Organic Chemistry: Principles and Mechanisms*, second edition. New York City: W.W. Norton & Company.

King, E. J. 1951. The Ionization Constants of Glycine and the Effect of Sodium Chloride upon Its Second Ionization. *J. Am. Chem. Soc* **73** (1): 155–159. https://doi.org/10.1021/ja01145a056.

Kiss, T., Sovago, I., and Gergely, A. 1991. Critical Survey of Stability Constants of Complexes of Glycine. *Pure and Applied Chemistry* **63** (4): 597–638. https://doi.org/10.1351/pac199163040597.

Korrani, A. K. N. and Jerauld, G. R. 2019. Modeling Wettability Change in Sandstones and Carbonates Using a Surface-Complexation-Based Method. *J Pet Sci Eng* **174**: 1093–1112. https://doi.org/10.1016/j.petrol.2018.12.016.

Kovscek, A. R., Wong, H., and Radke, C. J. 1993. A Pore-Level Scenario for the Development of Mixed Wettability in Oil Reservoirs. *AIChE J* **39** (6): 1072–1085. https://doi.org/10.1002/aic.690390616.

Lara Orozco, R. A., Abeykoon, G. A., Okuno, R. et al. 2021. The Impact of Glycine on the Zeta Potential of Calcite at Different Temperatures and Brine Compositions. *Colloids Surf, A Physicochem Eng Asp* **624**: 126851. https://doi.org/10.1016/j.colsurfa.2021.126851.

Lara Orozco, R. A., Abeykoon, G. A., Wang, M. et al. 2020. Amino Acid as a Novel Wettability Modifier for Enhanced Waterflooding in Carbonate Reservoirs. *SPE Res Eval & Eng* **23** (2): 741–757. SPE-195907-PA. https://doi.org/10.2118/195907-PA.

Liu, F. and Wang, M. 2020. Review of Low Salinity Waterflooding Mechanisms: Wettability Alteration and Its Impact on Oil Recovery. *Fuel* **267**: 117112. https://doi.org/10.1016/j.fuel.2020.117112.

Myint, P. C. and Firoozabadi, A. 2015. Thin Liquid Films in Improved Oil Recovery from Low-Salinity Brine. *Curr Opin Colloid Interface Sci* **20** (2): 105–114. https://doi.org/10.1016/j.cocis.2015.03.002.

Parkhurst, D. L. 1990. Ion-Association Models and Mean Activity Coefficients of Various Salts. In *Chemical Modeling of Aqueous Systems II*,Chap. 3, 30–43. Washington, DC: American Chemical Society.

Parkhurst, D. L. 1995. User's Guide to PHREEQC: A Computer Program for Speciation, Reaction-Path, Advective-Transport, and Inverse Geochemical Calculations (No. 95-4227). US Department of the Interior, US Geological Survey, Reston, Virginia.

Plummer, L. N. and Busenberg, E. 1982. The Solubilities of Calcite, Aragonite and Vaterite in CO2-H2O Solutions between 0 and 90°C, and an Evaluation of the Aqueous Model for the System CaCO3-CO2-H2O. *Geochim. Cosmochim. Acta* **46** (6): 1011–1040. https://doi.org/10.1016/0016-7037(82)90056-4.

Pokrovsky, O. S. and Schott, J. 2002. Surface Chemistry and Dissolution Kinetics of Divalent Metal Carbonates. *Environ. Sci. Technol.* **36** (3): 426–432. https://doi.org/10.1021/es010925u.

Pokrovsky, O. S., Schott, J., and Thomas, F. 1999. Dolomite Surface Speciation and Reactivity in Aquatic Systems. *Geochim. Cosmochim. Acta* **63** (19–20): 3133–3143. https://doi.org/10.1016/S0016-7037(99)00240-9.

Qiao, C., Johns, R., and Li, L. 2016. Modeling Low-Salinity Waterflooding in Chalk and Limestone Reservoirs. *Energy Fuels* **30** (2): 884–895. https://doi.org/10.1021/acs.energyfuels.5b02456.

Remko, M. and Rode, B. M. 2006. Effect of Metal Ions (Li+, Na+, K+, Mg2+, Ca2+, Ni2+, Cu2+, and Zn2+) and Water Coordination on the Structure of Glycine and Zwitterionic Glycine. *J Phys Chem A* **110** (5): 1960–1967. https://doi.org/10.1021/jp054119b.

Sanaei, A., Tavassoli, S., and Sepehrnoori, K. 2019. Investigation of Modified Water Chemistry for Improved Oil Recovery: Application of DLVO Theory and Surface Complexation Model. *Colloids Surf. A Physicochem* **574**: 131–145. https://doi.org/10.1016/j.colsurfa.2019.04.075.

Sharma, G. and Mohanty, K. K. 2013. Wettability Alteration in High-Temperature and High-Salinity Carbonate Reservoirs. *SPE J.* **18** (4): 646–655. SPE-147306-PA. https://doi.org/10.2118/147306-PA.

Sharma, H. and Mohanty, K. K. 2018. An Experimental and Modeling Study to Investigate Brine-Rock Interactions during Low Salinity Water Flooding in Carbonates. *J Pet Sci Eng* **165**: 1021–1039. https://doi.org/10.1016/j.petrol.2017.11.052.

Song, J., Rezaee, S., Zhang, L. et al. 2019. Characterizing the Influence of Organic Carboxylic Acids and Inorganic Silica Impurities on the Surface Charge of Natural Carbonates Using an Extended Surface Complexation Model. *Energy Fuels* **33** (2): 957–967. https://doi.org/10.1021/acs.energyfuels.8b03896.

Song, J., Zeng, Y., Wang, L. et al. 2017. Surface Complexation Modeling of Calcite Zeta Potential Measurements in Brines with Mixed Potential Determining Ions (Ca2+, CO32-, Mg2+, SO42-) for Characterizing Carbonate Wettability. *J Colloid Interface Sci* **506**: 169–179. https://doi.org/10.1016/j.jcis.2017.06.096.

Sørgård, H. N. and Seland, J. G. 2020. A Fluid Specific Dimension of Confinement as a Measure of Wettability in Porous Media. *J Magn Reson* **310**: 106663. https://doi.org/10.1016/j.jmr.2019.106663.

Takeya, M., Ubaidah, A., Shimokawara, M. et al. 2020. Crude Oil/Brine/Rock Interface in Low Salinity Waterflooding: Experiments, Triple-Layer Surface Complexation Model, and DLVO Theory. *J Pet Sci Eng* **188**: 106913. https://doi.org/10.1016/j.petrol.2020.106913.

Tetteh, J. T., Alimoradi, S., Brady, P. V. et al. 2020. Electrokinetics at Calcite-Rich Limestone Surface: Understanding the Role of Ions in Modified Salinity Waterflooding. *J Mol Liq* **297** (1): 111868. https://doi.org/10.1016/j.molliq.2019.111868.

Thomas, M. M., Clouse, J. A., and Longo, J. M. 1993. Adsorption of Organic Compounds on Carbonate Minerals: 1. Model Compounds and Their Influence on Mineral Wettability. *Chem. Geol.* **109** (1–4): 201–213. https://doi.org/10.1016/0009-2541(93)90070-Y.

Tripathy, D. B., Mishra, A., Clark, J. et al. 2018. Synthesis, Chemistry, Physicochemical Properties and Industrial Applications of Amino Acid Surfactants: A Review. *C. R. Chim* **21** (2): 112–130. https://doi.org/10.1016/j.crci.2017.11.005.

Van Cappellen, P., Charlet, L., Stumm, W. et al. 1993. A Surface Complexation Model of the Carbonate Mineral-Aqueous Solution Interface. *Geochim. Cosmochim. Acta* **57** (15): 3505–3518. https://doi.org/10.1016/0016-7037(93)90135-J.

Wales, D. J. and Doye, J. P. K. 1997. Global Optimization by Basin-Hopping and the Lowest Energy Structures of Lennard-Jones Clusters Containing Up to 110 Atoms. *J. Phys. Chem. A* **101** (28): 5111–5116. https://doi.org/10.1021/jp970984n.

Wang, P., Oscarson, J. L., Gillespie, S. E. et al. 1996. Thermodynamics of Protonation of Amino Acid Carboxylate Groups from 50 to 125°C. *J Solution Chem* **25** (3): 243–266. https://doi.org/10.1007/BF00972523.

Yousef, A. A., Al-Saleh, S., and Al-Kaabi, A. 2011. Laboratory Investigation of the Impact of Injection-Water Salinity and Ionic Content on Oil Recovery From Carbonate Reservoirs. *SPE Res Eval & Eng* **14** (5): 578–593. https://doi.org/10.2118/137634-PA.

Zhang, P., Tweheyo, M. T., and Austad, T. 2007. Wettability Alteration and Improved Oil Recovery by Spontaneous Imbibition of Seawater into Chalk: Impact of the Potential Determining Ions Ca2+, Mg2+, and SO42−. *Colloids Surf, A Physicochem Eng Asp* **301** (1–3): 199–208. https://doi.org/10.1016/j.colsurfa.2006.12.058.